

Robust helical edge transport at $\nu = 0$ quantum Hall state

G. M. Gusev,¹ D. A. Kozlov,^{2,3} A. D. Levin,¹ Z. D. Kvon,^{2,3} N. N. Mikhailov,² and S. A. Dvoretzky,²

¹*Instituto de Física da Universidade de São Paulo, 135960-170, São Paulo, SP, Brazil*

²*Institute of Semiconductor Physics, Novosibirsk 630090, Russia and*

³*Novosibirsk State University, Novosibirsk 630090, Russia*

(Dated: August 19, 2021)

Among the most interesting predictions in two-dimensional materials with a Dirac cone is the existence of the zeroth Landau level (LL), equally filled by electrons and holes with opposite chirality. The gapless edge states with helical spin structure emerge from Zeeman splitting at the LL filling factor $\nu = 0$ gapped quantum Hall state. We present observations of a giant nonlocal four-terminal transport in zero-gap HgTe quantum wells at the $\nu = 0$ quantum Hall state. Our experiment clearly demonstrates the existence of the robust helical edge state in a system with single valley Dirac cone materials.

Two dimensional massless Dirac fermions in the presence of a strong perpendicular magnetic field show several remarkable features that sharply diverge from conventional behaviour [1-8]. The energy spectrum is organized in Landau levels (LL) with square root versus linear dependence on the magnetic field and square root dependence on the Landau index n versus $n + 1/2$, in comparison with the parabolic dispersion at the zero field. The most remarkable consequence of this last property is the existence of a zero-energy Landau level ($n = 0$). This is not due to the linear spectrum, but is related to the π Berry phase carried by each Dirac point. Therefore, the $n = 0$ LL has a magnetic field independent energy, which is quite different from a quantized cyclotron orbit in the conventional quantum Hall effect. It is important to find the clear experimental signature that can help to identify zeroth Landau level in many Dirac materials, such as graphene [2], three-dimensional topological insulators [9] and Weyl semimetals [10].

The existence of the zeroth Landau level has been examined by measurements of the integer quantum Hall effect (QHE) in graphene [2]. Previous experiments in samples with moderate mobility provide indirect evidence of the QHE around filling factor $\nu = 0$: the Hall conductivity has a peculiar plateau at $\sigma_{xy} = 0$ that is not precisely quantized as other plateaus are, and its longitudinal resistivity does not vanish [11]. But this interpretation is based on the bulk spectrum scenario (figure 1a). Note, however, that understanding of the QHE at $\nu = 0$ requires a presence of edge states similar to the conventional integer QHE. In this case, the interpretation becomes ambiguous and depends on the particular structural properties of graphene. In particular, one of the scenarios predicts that, if spin splitting is larger than valley splitting, the bulk Landau level forms two counter propagating edge states [12] similar to 2D topological insulators [13] as shown in Figure 1b. It is worth noting that unambiguous experimental support for the existence of counter-propagating edge states is provided by nonlocal measurements. The helical edge state transport at $\nu = 0$ differs from the chiral edge mode transport for a higher LL: chiral states carry the same chemical potential in the vicinity of each boundary, while counter circulating

edge states carry potential from different current probes (left and right). As a result, conductance is zero in the QHE regime and quantized in universal units $2e^2/h$ in the QH-metal regime in the absence of backscattering between spin-polarized states. Several attempts have been made to study nonlocal transport in graphene, however, opposing or conflicting interpretations have been offered [14,15]. Very recently observation of the quantized local and nonlocal resistances in a single layer [16] and in bilayer [17] graphene of micrometer-sized samples in the presence of the strong in-plane magnetic field has been reported, which has been attributed to the parallel B-induced helical edge modes. Application of other materials that possess a single Dirac cone is of particular interest.

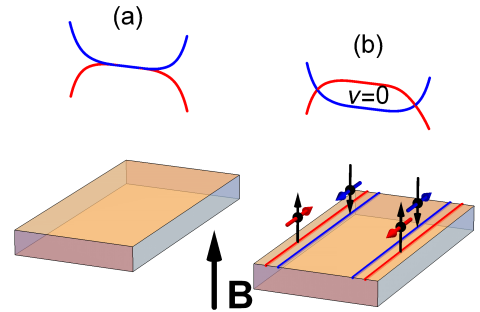


FIG. 1: (Color online) Schematics of band structure (energy spectrum) in low (a) and high (b) magnetic field, showing the zero LL in the middle of the sample and at the sample edge, and counter propagating spin polarized edge states in a slab-shaped sample for the $\nu = 0$ LL state.

Recently a two-dimensional system with a single Dirac cone spectrum, based on HgTe quantum wells, has been discovered [18,19]. The single spin degenerate Dirac val-

ley allows unambiguous identification of the features resulting from the bulk zeroth Landau level. In addition, the high mobility and giant Lande g-factor (~ 55) favor formation of spin-polarized counter-propagating states. In the present paper, we studied the nonlocal transport in 10-probe devices fabricated from HgTe zero-gap quantum structures. We observe a magnetic field induced, giant, nonlocal resistance peak near the CNP in different configurations of current and voltage probes. The nonlocal response is comparable with local resistance and increases rapidly with B. The nonlocal resistance persists in magnetic fields up to 7 T. Simple Kirchhoff based estimations and more complicated edge state+bulk model calculations clearly confirm the existence of helical edge states originating from the bulk zeroth LL.

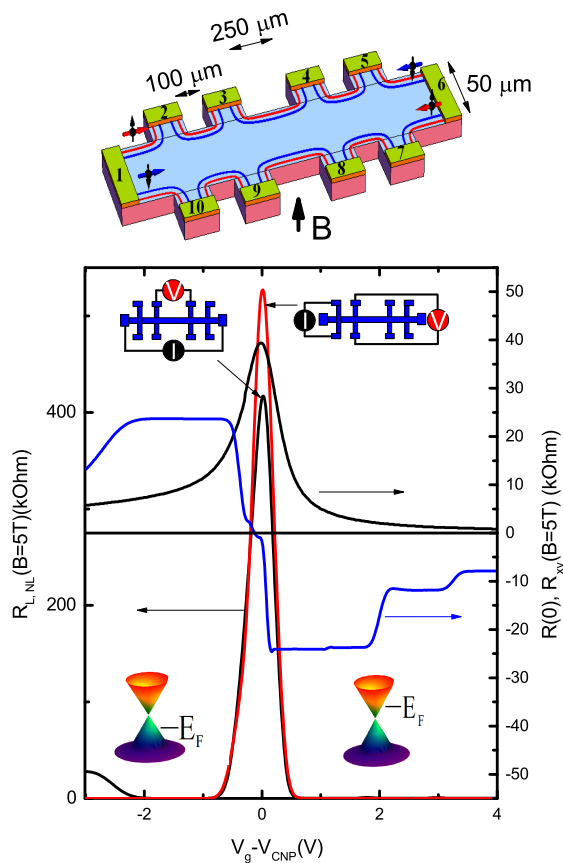


FIG. 2: (Color online) Top-a schematic of device (not preserving aspect ratio) and the local zero field resistance $R(0)$, longitudinal $R_L = R_{xx}$ ($I=1,6$, $V=3,4$) (black curve) Hall R_{xy} ($I=1,6$; $V=3,9$) (blue curve) and nonlocal R_{NL} ($I=2,10$; $V=3,9$) (red curve) resistances as a function of gate voltage at $B=5$ T, $T=4.2$ K, $I = 10^{-9}$ A. The schematics show how the current source and the voltmeter are connected for the measurements.

Quantum wells $Cd_{0.65}Hg_{0.35}Te/HgTe/Cd_{0.65}Hg_{0.35}Te$ with (013) surface orientations and a well thickness of 6.3, 6.4 and 6.6 nm were prepared by molecular beam epitaxy. A detailed description of the sample structure

has been given in Refs. [17,18]. The sample is a Hall bar device with 8 voltage probes. The bar has a width W of $50\mu m$ and three consecutive segments of different lengths L ($100, 250, 100\mu m$) (fig.2). A dielectric layer was deposited (100 nm of SiO_2 and 100 nm of Si_3Ni_4) on the sample surface and then covered by a TiAu gate. The density variation with gate voltage was $1 \times 10^{11} cm^{-2} V^{-1}$. The magnetotransport measurements were performed in the temperature range $1.4 - 70K$ using a standard four point circuit with a $1 - 13Hz$ ac current of $1 - 10nA$ through the sample, which is sufficiently low to avoid overheating effects. It is worth noting that the electrical contacts to the electron gas beneath the gate electrode become worse in a strong magnetic field, therefore we report the results up to 5 or 7 T (depending on the particular device). 10 devices from three different wafers were measured, all with similar results.

Figure 2 shows the zero field, longitudinal R_{xx} , Hall R_{xy} and nonlocal R_{NL} resistances measured in a perpendicular magnetic field $B=5$ T as a function of gate voltage. R_{xx} and R_{xy} are measured in multiterminal Hall bar geometry. In the local configuration, the current flows between contacts 1,6 and voltage is measured between probes 3,4 ($R_L = R_{xx} = R_{1-6,3-4} = V_{3,4}/I_{1,6}$) and Hall voltage is measured between probes 3,9 ($R_{xy} = R_{1,6}^{3,9} = V_{3,9}/I_{1,6}$). In the nonlocal configuration, the current flows between contacts 2,10 and voltage is measured between probes 3,9 ($R_{NL} = R_{2,10}^{3,9} = V_{3,9}/I_{2,10}$). Zero field resistance behaviour resembles behaviour in other HgTe-based quantum wells, including topological insulators [13,19,20] and semimetals [23,24]: resistance shows a peak around the charge neutrality point (CNP). In graphene and zero gap HgTe wells, the CNP is coincident with the Dirac point [5,7,18,19]. The maximum resistivity at the Dirac point $\rho_{xx} = \frac{W}{L} R_{1,6}^{3,4}(0) = 0.3 \frac{h}{e^2}$ agrees with others' observations [18,20].

When we applied an external perpendicular magnetic field a pronounced anomaly in the resistance data was observed: resistance was found to increase very strongly with B near the CNP, while in other regions the system demonstrates conventional quantum Hall behaviour (fig.2). Evolution of the local $R_L = R_{1,6}^{3,4} = V_{3,4}/I_{1,6}$ and nonlocal $R_{NL} = R_{2,10}^{3,9} = V_{3,9}/I_{2,10}$ resistances with gate voltage and magnetic field is shown in Figure 3. Both R_L and R_{NL} exhibit sharp peaks above the critical magnetic field $B_c \sim 2.5T$. Nonlocality is absent in the magnetic field below B_c .

The important difference between the quantum Hall states with $\nu = 0$ and $\nu \neq 0$ is that, in the conventional quantization regime, the longitudinal transport coefficient vanishes in both conductivity σ_{xx} and resistivity ρ_{xx} , while for the QHE state in $\nu = 0$ this is not necessarily the case $\rho_{xx} = 0$. Indeed we obtain $\sigma_{xy} \sim \sigma_{xx} \sim 0$ because $\rho_{xx} \gg \rho_{xy}$ at $\nu = 0$ [23]. Note that for the Hall insulating state it is expected that both longitudinal and Hall resistivities are going to infinity near the CNP

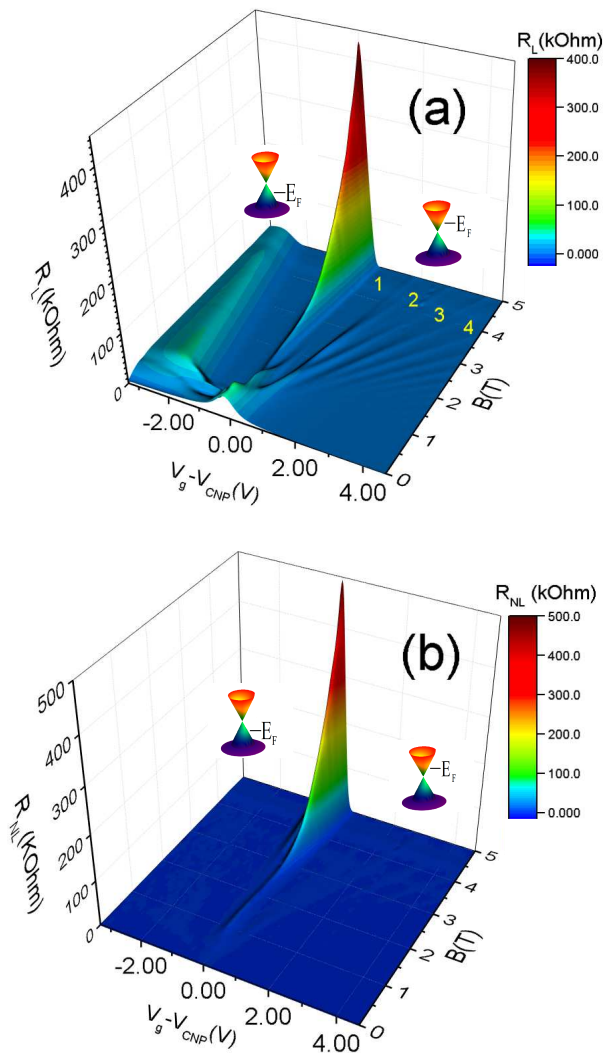


FIG. 3: (Color online) The local $R_L = R_{xx}$ ($I=1,6$, $V=3,4$) (a) and nonlocal R_{NL} ($I=2,10$; $V=3,9$) (b) resistances as a function of the gate voltage and magnetic field, $T=4.2$ K. Filling factors determined from Hall resistance are labeled.

in accordance with the classical Hall resistivity formula $\rho_{xy} \sim B/(n-p)ec$, where n and p are electron and hole densities respectively, if we assume the same mobility for both carrier types. Divergent longitudinal and vanishing Hall resistivities have been observed at the Dirac point in graphene and attributed to density inhomogeneities associated with electron-hole puddles [26]. The alternative approach to the $\nu = 0$ quantum Hall effect was based on counter-propagating edge channels with opposite spin directions [12]. In this model the Hall resistance is zero because of compensation between the helical states in accordance with Landauer-Buttiker formalism, while the resistance measured between probes is quantized in units of $h/2e^2$ in the ballistic case and much higher than the resistance quantum in the diffusive case, similar to a 2D

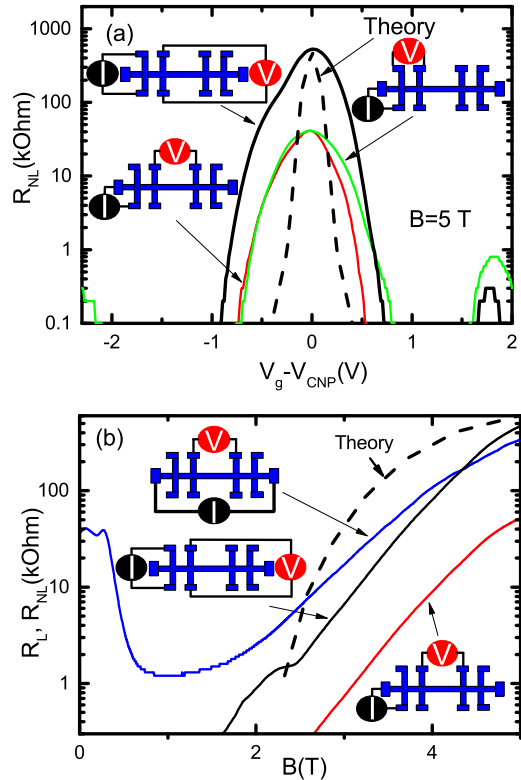


FIG. 4: (Color online)(a) The nonlocal R_{NL} resistances as a function of gate voltage at $B=5$ T, $T=4.2$ K, obtained for different measuring configurations. Dashes - nonlocal resistance R_{NL} ($I=2,10$; $V=3,9$) calculated from model [23]. (b) Comparison of the magnetic field dependencies for both local and nonlocal resistances in various configurations obtained at the CNP. Dashes - nonlocal resistance R_{NL} ($I=2,10$; $V=3,9$) calculated from model [23]. The schematics show how the current source and the voltmeter are connected for the measurements.

topological insulator in zero magnetic field [22,27].

We provide new evidence that advances this debate by measuring the long range nonlocal transport in the quantum Hall effect regime in Dirac cone materials. For example, because graphene has two valleys, two different situations must be considered, depending on whether the bulk valley splitting is larger or smaller than the bulk spin splitting in the zeroth LL. If the valley degeneracy lifts first, and valley separation becomes larger than the Zeeman energy, the edge states do not cross and the gap appears both in the bulk and at the edges of the sample. Such a quantum Hall insulator resembles common insulators without edge states. The other possibility occurs when the Zeeman energy is larger than the valley splitting. The electron-like (hole-like) Landau level bends upwards (downwards) in energy near the edge of the sample and forms two counter-propagating edge states residing

on the same edge (figure 1b). Such QH-metal resembles a nontrivial topological insulator in a zero magnetic field with a bulk gap and helical edge states protected by the time reversal symmetry against backscattering [13]. The mechanism of the lift of fourfold degeneracy and the existence of a possible insulating state in graphene have been discussed extensively [28-32]. A high-field insulating state has been observed in both low and high quality graphene samples. The general consensus is that the magnetic field drives graphene at the CNP from the QH-metal state at a relative low field into the QH-insulator state at a high enough field. Note, however, the presence of electron-hole puddling due to inhomogeneity can mask metallic behaviour at low magnetic fields and observation of the B-independent resistance peak may not be sufficient for the actual manifestation of the zeroth LL.

Figure 4a illustrates R_{NL} for various configuration measured at a fixed magnetic field $B=5T$. Figure 4b shows the magnetic field dependence of both local and nonlocal resistances at fixed gate voltage corresponding to the CNP. One can see almost exponential growth of R_L and R_{NL} above B_c . In the magnetic field region $0.3T < B < 1.4T$, the experimental local resistance shows complex and diverse behaviour: it reveals a large negative magnetoresistance and plateaux-like features. Previously [20] these features have been attributed to the emergence of the zeroth Landau level without edge states (see figure 1a), which is represented by a sharp peak near the CNP in $\sigma_{xx}(V_g)$. When the magnetic field is such that the bulk Zeeman gap is larger than the zeroth LL broadening Γ , which occurs at $B_c \approx \Gamma/g\mu_B \approx 2.5T$, where μ_B is the Bohr magneton, one expects nonlocal transport due to the helical edge states. The nonlocal resistance is strongly suppressed at high temperatures, while the local resistance is found to be much more robust [27].

To get more insight into the physics of the observed nonlocality, it is important to estimate the phenomenon theoretically. To explain the value of the local and nonlocal resistances in most of the experimental observations mentioned above, a simple picture of the helical edge state is usually enough. We have seen that, using Kirchhoffs laws, we can analyze our circuit. There is a simple expression that allows one to calculate the resistance value for any measurement configuration assuming that there is only edge state transport in the sample [27]: $R_{n,m}^{i,j} = \frac{L_{n,m}L_{i,j}}{Ll}(h/e^2)$, where $R_{n,m}^{i,j}$ is the voltage measured between contacts i and j while the current is maintained between contacts n and m , $L_{i,j}$ ($L_{n,m}$) are the distances between i and j (n and m) along the gated sample edge that does not include n and m (i and j), L is the total perimeter of the sample, and l is the mean free path due to the scattering between helical states propagated along the same edge. Assuming a homogeneous material and that the mean path remains constant along the edge, we obtain the ratio between nonlocal and local resistances: $R_{NL}/R_L = R_{2,10}^{3,9}/R_{1,6}^{3,4} = 2$;

$R_{NL}/R_L = R_{1,10}^{2,3}/R_{1,6}^{3,4} = 0.11$; $R_{NL}/R_L = R_{1,10}^{3,4}/R_{1,6}^{3,4} = 0.125$. The result of these calculations is close to the experimental result: $(R_{NL}/R_L)^{exp} = R_{2,10}^{3,9}/R_{1,6}^{3,4} = 1.1 - 1.75$; $(R_{NL}/R_L)^{exp} = R_{1,10}^{2,3}/R_{1,6}^{3,4} = 0.08 - 0.1$; $(R_{NL}/R_L)^{exp} = R_{1,10}^{3,4}/R_{1,6}^{3,4} = 0.07 - 0.1$. There is an interesting fact that, in certain sample probe configurations, one can obtain a nonlocal resistance greater than the local one (figs.2,3).

However, away from the CNP, the current penetrates into the interior of the sample, and the system behaves more and more like a conventional two-dimensional gas. We apply formalism developed in Ref.10 to describe the local resistance in graphene near $\nu = 0$ in QH metal and then extended it to nonlocal resistance in semimetals [33]. The model explains the transport coefficients in the regime, where the edge-state current is suppressed by bulk contribution to conductivity. The scattering between the edge states and the scattering between bulk states and each of the edge states is characterized by the mean free path $\gamma^{-1} = l$ and g^{-1} respectively, which are assumed to be smaller than the sample's dimensions [25].

Figs.4 a,b display the results obtained from this model for typical parameter values $\gamma^{-1} = 0.33\mu m$ and $g^{-1} = 0.33\mu m$. Clearly, the model reproduces qualitatively the main features of the measurements, in particular, suppression of the peak away from the CNP by bulk contribution to the transport and rapid growth with the magnetic field due to Zeeman splitting. Note that calculated peak profile is sharper than the measured one. A detailed comparison with the experiment requires knowledge of the density of the states in the gap between the Landau levels, and ratio between localized and delocalized electrons on the tails of the Gaussian density of states in the quantum Hall regime.

A number of the theoretical models have addressed the evolution of the helical edge states in a magnetic field [34-36]. The results appear to be controversial: while primary models predict that the counter propagating edge states persist up to a critical magnetic field [34,35], more recent calculations demonstrate the emergence of a gap in the spectrum of the edge states at an arbitrary small B [36]. Such high sensitivity of the edge state spectrum to the external magnetic field has been attributed to the natural interface inversion asymmetry in HgTe quantum wells. In sharp contrast with this prediction, we observe a giant nonlocal magnetoresistance, which confirms the persistence of the helical states up to 7 T. Note that the effective Hamiltonian which ascribes the bulk energy spectrum and the structure of the edge states in the presence of the perpendicular magnetic field is not properly derived from microscopic theory. For example, other 6×6 matrix Hamiltonian has been successfully applied to the calculation of the energy spectrum in HgTe quantum wells in the presence of an in-plane magnetic field [37]. Further theoretical study is required.

In conclusion, we have studied the local and nonlocal transport properties of the zero Landau level in a Dirac cone 2D system based on a zero-gap HgTe quantum well.

A giant, nonlocal resistance has been observed at the $\nu = 0$ quantum Hall effect. In comparison with graphene, which is the most typical 2D material with Dirac cones, our system has several advantages. Firstly, the single cone spectrum allows unambiguous interpretation of the integer Hall effect based on the existence of counterpropagating edge states with opposite spin emerging from the zero bulk LL, ruling out the valley first split model in graphene. Secondly, the advantage in fabrication (MBE growth versus exfoliation) allows the production of samples with a large distance between probes and, therefore, justifies the long range nature of the nonlocal transport due to the edge states.

The financial support of this work by the Russian Science Foundation (Grant No. 16-12-10041, MBE growth of HgTe QWs, fabrication of the field effect transistors and carrying out of the experiment and data analysis), FAPESP (Brazil) and CNPq (Brazil) is acknowledged. The authors thank O. E. Raichev for helpful discussions.

I. ONLINE SUPPLEMENTAL MATERIAL TO : ROBUST HELICAL EDGE TRANSPORT AT $\nu = 0$ QUANTUM HALL STATE

A. Resistivity and conductivity tensors and $R_{xx}(B, n_s)$ diagram

In the main text, we demonstrate the magnetoresistance and Hall effect as a function of the gate voltage at a fixed magnetic field. Longitudinal resistance reveals a giant peak near the CNP with values $R_{xx} \gg h/e^2$, and the Hall effect demonstrates bipolar behaviour. Sometimes it is instructive to convert the resistivities to a conductivity tensor through a matrix inversion. The quantum Hall state with $\nu = 0$ distinguishes states with $\nu \neq 0$. For example, in the conventional quantization regime, the longitudinal transport coefficient vanishes in both conductivity σ_{xx} and resistivity ρ_{xx} , while for the QHE state in $\nu = 0$ the longitudinal resistance shows maxima rather than minima and $\rho_{xx} \gg \rho_{xy}$. Figure 5a shows transport coefficients in zero magnetic field and at $B=7$ T as a function of gate voltage. Indeed we obtain $\sigma_{xy} \sim \sigma_{xx} \sim 0$ because $\rho_{xx} \gg \rho_{xy}$ at $\nu = 0$, as is shown in Figure 5b. Most importantly, however, this does not prove the existence of the Hall insulating state, and further measurements of the nonlocal transport is required. The results of such measurements are presented in the main text. Because the resistance peak at the CNP is larger than the magnetoresistance oscillations related to higher Landau levels, it is convenient to visualize the quantum Hall effect through a $R_{xx}(B, n_s)$ diagram.

Figure 6 displays the evolution of longitudinal resistance with a magnetic field and density ($R_{xx}(B, n_s)$). One can see stripes corresponding to resistance maxima and minima in the $B - n_s$ plane for electron-like states. It is worth noting that there is no direct correspondence between the experimental $R_{xx}(B, n_s)$ plot and the LL spec-

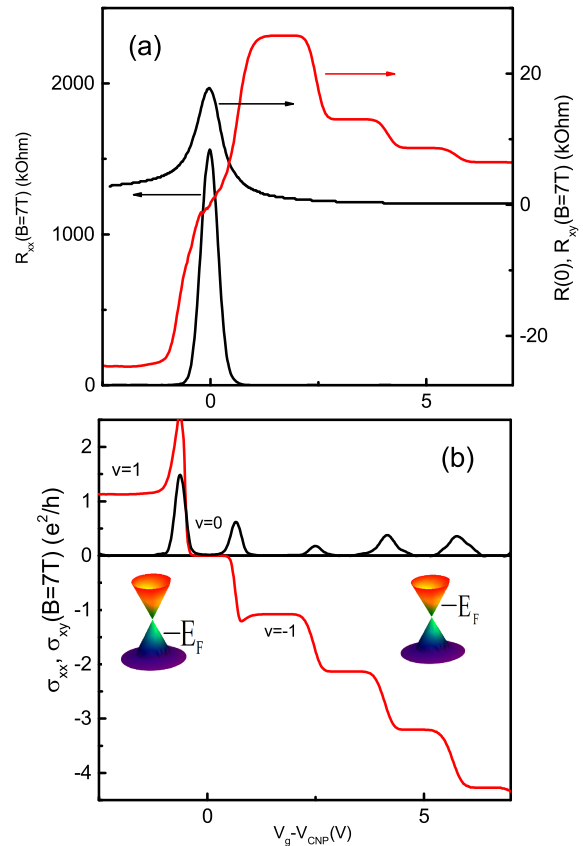


FIG. 5: (Color online) (a) The local zero field resistance $R(0)$, longitudinal $R_L = R_{xx}$ ($I=1,6$, $V=2,3$)(black curve) and Hall R_{xy} ($I=1,6$; $V=3,9$)(red curve) resistances as a function of gate voltage at $B=7$ T, $T=4.2$ K, $I = 10^{-9}$ A. (b) The longitudinal and Hall conductivities as a function of gate voltage at $B=7$ T.

trum because of the oscillating behaviour of Fermi energy. The Dirac LL spectrum has a square root dependence on the magnetic field, while the experimental $R_{xx}(B, n_s)$ diagram shows a linear n_s versus B dependence, where slopes of the stripes are determined by the LL filling factors ν : $\frac{dB}{dn} = \frac{\nu e}{h}$. Filling factors determined from the slopes are coincident with those determined from the Hall resistance.

B. Edge and bulk transport model and comparison with experiment

The mechanism responsible for the observed sharp peak of the local and nonlocal resistivities near the charge neutrality point (CNP) in zero gap HgTe quantum wells relies on the combination of the edge state and bulk transport contributions with account of the backscattering within one edge as well as bulk-edge coupling. When the gate voltage is swept through the CNP, the local and nonlocal transport coefficients arise from the edge state

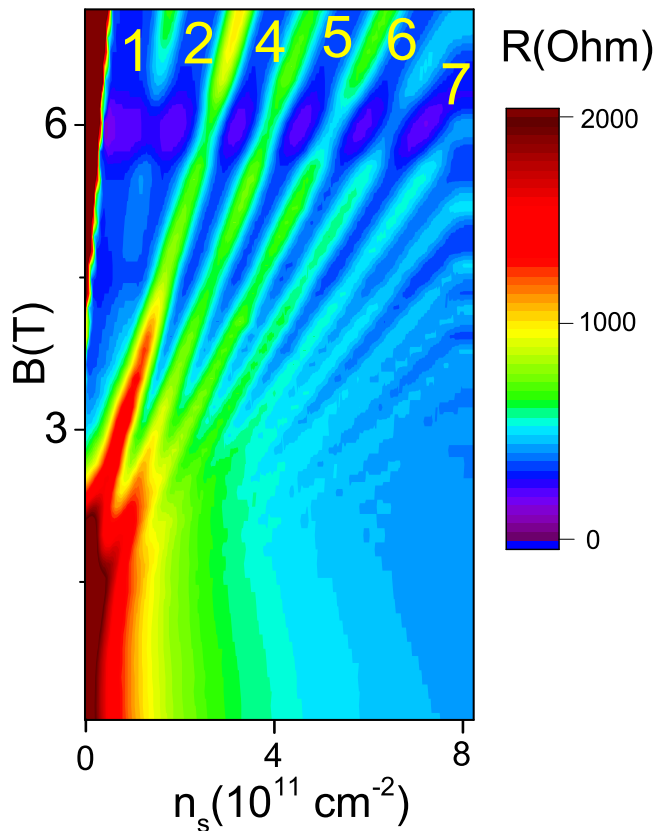


FIG. 6: (Color online) (a) $R_{xx}(B, n_s)$ diagram, $T=4.2$ K. Filling factors $|\nu|$ determined from Hall resistance are labeled.

contribution at the CNP and the short-circuiting of the edge transport by the bulk contribution away from the CNP.

Our analysis of transport coefficients in the main text was based on a simplified model developed for the explanation of the quantum Hall effect state in graphene at $\nu = 0$, when the spin degeneracy is lifting before valley splitting [12]. Within this scenario, the transport in graphene in a strong magnetic field is dominated by a pair of gapless counter propagating chiral edge modes with opposite spin. The transport properties in the bulk can be described by the current-potential relation

$$\mathbf{j}_i = -\hat{\sigma}_i \nabla \psi_i, \quad (1)$$

$$\hat{\sigma}_i = \begin{pmatrix} \sigma_{xx}^{(i)} & \sigma_{xy}^{(i)} \\ -\sigma_{xy}^{(i)} & \sigma_{xx}^{(i)} \end{pmatrix}, i = 1, 2$$

where $\psi_{1,2}$ are the electrochemical potentials for electron-like and hole-like states. So we can solve the

problem by solving the Laplace equation for these potentials $\nabla^2 \psi_{1,2} = 0$ because of the charge conservation continuity conditions $\nabla \cdot \mathbf{j}_i = 0$. A solution to Laplace's equation is uniquely determined if the value of the function is specified on all boundaries. In order to describe the transport properties in the presence of the edge states, we introduce two phenomenological constants γ and g , which represent edge to edge and bulk to edge inverse scattering length respectively. The boundary conditions describing the bulk edge coupling are given by

$$\mathbf{n} \cdot \mathbf{j}_i = g(\psi_i - \varphi_i), \quad (2)$$

where \mathbf{n} is a normal vector to the boundary, φ_i are local chemical potentials of the electron-like and hole-like edge states.

The edge state transport can be described by the equations for particle density [12], taking into account the scattering between the edge and the bulk

$$\partial_x \varphi_1 = \gamma(\varphi_2 - \varphi_1) + g(\psi_1 - \varphi_1), \quad (3)$$

$$-\partial_x \varphi_2 = \gamma(\varphi_1 - \varphi_2) + g(\psi_2 - \varphi_2), \quad (4)$$

Another couple of similar equations describe the variables $\varphi_{1'}$ and $\varphi_{2'}$ at the opposite edge.

The general solution of this problem, therefore, includes the solution of the 2D Laplace equation for the bulk electrochemical potentials $\psi_{1,2}$ together with 8 equations (2,3,4) describing the scattering between electron-like and hole-like edge states and between the edge and bulk states. The current can be calculated from this solution as a sum of the contribution from the bulk and both edge states. We assumed that the bulk conductivities for electrons and holes are represented by Gaussians in e^2/h units

$$\sigma_{xx}^{(1)} = e^{-\left(\frac{E-\mu}{\Gamma}\right)^2}, \sigma_{xx}^{(2)} = e^{-\left(\frac{E+\mu}{\Gamma}\right)^2}, \quad (5)$$

where the parameter Γ is the width of the Landau level (LL), $E = \frac{g\mu_B B}{2}$ is Zeeman splitting, μ is the electrochemical potential. In the Gaussian models, the Landau level width is proportional to $B^{1/2}$. Because Zeeman valley splitting is not well known, we can rewrite equations (5) in terms of the LL filling factor ν [1]:

$$\sigma_{xx}^{(1,2)} = e^{-A(\nu \pm 1)^2} \quad (6)$$

The Hall conductivities are determined from the semi-circle relation

$$\sigma_{xy}^{(1,2)}(\sigma_{xy}^{(1,2)} \mp 2) + (\sigma_{xx}^{(1,2)})^2 = 0 \quad (7)$$

The full edge + bulk model in the local resistance configuration can be solved either analytically or numerically. The analytical solution has been obtained in Ref.12 for graphene. It is worth noting that the model describes the local resistance behaviour as a function of energy. A detailed comparison with the experiment requires knowledge of the density of the states in the gap between the

Landau levels because the Fermi energy does not vary linearly within the bulk gap region. In the absence of disorder, the Fermi level jumps from the electron-like LL to the hole-like LL, and a sharp resistance peak is expected, in contrast to the broad maximum observed in the experiment. The existence of metallic puddles could be responsible for a smoother Fermi level displacement, similar to graphene. For simplicity's sake, we can assume that the fraction of the puddles between the LL is constant, which leads to a constant density of states inside the bulk gap D_0 . Comparing the energy and the density scales, we obtain $D_0 = 0.8 \times 10^{10} \text{ cm}^{-2} \text{ meV}^{-1}$. Electrons in the puddles are localized and do not contribute to conductivity.

The edge + bulk model in the nonlocal resistance configuration can only be solved by numerical methods. We have performed a self consistent calculation to find the $\psi_{1,2}$ solution of the Laplace equation in two space dimensions and the $\varphi_{1,2}$ solutions of equations 3 and 4 on the edge of the Hall bar. The equations for $\psi_{1,2}$ are discretized by the Finite Element Method. Dirichlet boundary conditions are set at $50 \mu\text{m}$ wide metal contacts located at the left and right side of the bar for the local case or $10 \mu\text{m}$ wide contacts around $x = 0$ at the top and bottom edge of the bar for the non-local case. The generalized Neumann boundary conditions (eq 2) are set everywhere else. To solve the boundary value problem for a system of ordinary differential equations 3 and 4 we use a finite difference code that implements the 3-stage Lobatto IIIa formula. The boundary conditions are set to $\varphi_{1,2} = \psi_{1,2}$ inside the metal contacts. Resistance for the non-local case is calculated as

$$\begin{aligned}
 R_{xx} &= V I_{tot}^{-1}, \quad I_{tot} = I_{edge} + I_{bulk}, \\
 V &= \frac{1}{2} (\varphi_{11} - \varphi_{11'} + \varphi_{21} - \varphi_{21'}), \\
 I_{edge} &= \varphi_1 - \varphi_2 + \varphi_{2'} - \varphi_{1'}, \\
 I_{bulk} &= \sigma_{xy}^{(1)} (\psi_1 - \psi_{1'}) - \sigma_{xx}^{(1)} \int \frac{\partial \psi_1}{\partial y} dx + \\
 &\quad \sigma_{xy}^{(2)} (\psi_2 - \psi_{2'}) - \sigma_{xx}^{(2)} \int \frac{\partial \psi_2}{\partial y} dx, \quad (8)
 \end{aligned}$$

where V is the non-local potential difference, I_{tot} is the total current flowing between contacts, I_{edge} is the current flowing on the edge, I_{bulk} is the current flowing through the 2D layer, φ_{i1} and $\varphi_{i1'}$ are the potentials at the probe locations on the top and bottom edge correspondingly, φ_i , ψ_i , and $\varphi_{i'}$, $\psi_{i'}$ are the potentials at the opposite edges. For the local resistance configuration, all the potentials are calculated in a similar way, but the variables for derivative and integration in the equation for I_{bulk} are interchanged. These give results entirely in agreement with those found from the analytical solutions (Ref.12). In summary, we provide the details of our modeling for the local and non-local resistance as a function of carrier density N_s , which we used to produce Fig. 4 in the main

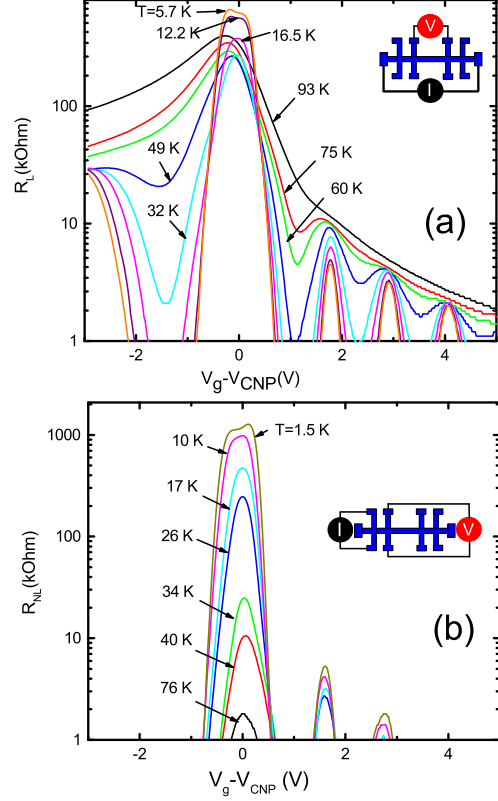


FIG. 7: (Color online) The local $R_L = R_{xx}$ ($I=1,6$, $V=3,4$) (a) and nonlocal R_{NL} ($I=2,10$; $V=3,9$) (b) resistances as a function of the gate voltage and temperature, $B=5$ T. The schematics show how the current source and the voltmeter are connected for the measurements.

text. We focus on the QHE regime ($B = 5$ T; $T = 4.2$ K). The best agreement between the experiment and theory is reached for a value of the Landau level broadening for electron-like and hole-like states $A=13$, $\gamma^{-1} = 0.33 \mu\text{m}$ and $g^{-1} = 0.33 \mu\text{m}$. The magnetic field dependence of the nonlocal resistance has been modeled from variation of Γ (or A) with B , taken into account that the Zeeman splitting between LL peaks proportional to B . The modeled behavior of the local and non-local resistivity is consistent with our experimental observations. Note that the model we consider is fairly phenomenological, and it is only valid at very low, ideally zero temperature. Note, however, that model reproduced many observed features, in particular, peak values, magnetic field and density dependencies.

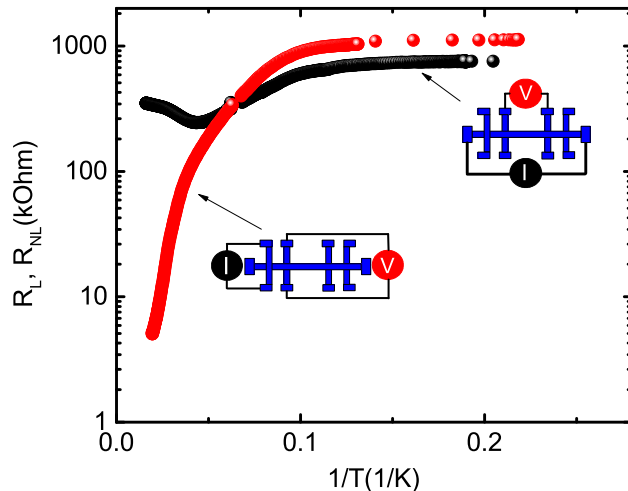


FIG. 8: (Color online) The local $R_L = R_{xx}$ ($I=1,6$, $V=3,4$) and nonlocal R_{NL} ($I=2,10$; $V=3,9$) resistances at CNP as a function of the inverse temperature, $B=5$ T. The schematics show how the current source and the voltmeter are connected for the measurements.

C. Temperature dependence of the local and nonlocal resistances in the presence of the magnetic field

In order to better understand the origin of the magnetic field induced nonlocality near CNP we studied the temperature dependence of R_{NL} and R_L . Figure 7 shows the evolution of local (a) and nonlocal (b) resistances

voltage profiles with temperature. There is obvious difference in the behaviour of the two signals: the peak in R_{NL} at CNP dramatically decreases above $T > 10K$, while local resistance peak is saturated at $T \approx 30K$ and starts to rise at the higher temperature. The different temperature regimes are more clearly revealed in the Figure 8. At low T both peaks in R_{NL} and R_L decrease slowly with increasing T, whereas above $\sim 10K$, one can see exponential decrease in both signals. Above $T > \sim 30K$ peak in R_{NL} follows a continuous exponential decay, while local signal changes from decreasing to increasing.

There are a number of physical mechanisms that can be responsible for the temperature dependence of the local and nonlocal resistance at the CNP. First, the nonlocal resistance can be suppressed, because the charge carriers from localized states in Landau level tails are thermally excited into delocalized states and contribute to conductivity, which shunts the edge state transport at high temperature. Second, parameters γ and g are expected to be temperature dependent. In general, determination of local and nonlocal resistances requires a detailed knowledge of the distribution functions at finite temperature, found from a system of kinetic equations including both elastic and inelastic scattering. In the presence of edge to bulk coupling, this problem is very complicated and out of scope of this paper. In the simplified case, however, we could estimate that the nonlocal resistance drops in 3 order of magnitude, assuming that the LL broadening increases in 1.3-1.5 times at highest temperature ($\sim 70K$), which reasonably agrees with our observations (Figs 7 and 8).

-
- [1] K. S. Novoselov, A. K. Geim, S. V. Morozov, D. Jiang, Y. Zhang, S. V. Dubonos, I. V. Grigorieva, A. A. Firsov, *Science* **306**, 666 (2004).
 - [2] K. S. Novoselov, A. K. Geim, S. V. Morozov, D. Jiang, M. I. Katsnelson, I. V. Grigorieva, S. V. Dubonos and A. A. Firsov, *Nature* **438**, 197 (2005); Y. Zhang, Y.-W. Tan, H. L. Stormer and P. Kim, *Nature* **438**, 201 (2005).
 - [3] K. S. Novoselov, E. McCann, S. V. Morozov, V. I. Fal'ko, M. I. Katsnelson, U. Zeitler, D. Jiang, F. Schedin and A. K. Geim, *Nat. Phys.* **2**, 177, (2006).
 - [4] K. S. Novoselov, Z. Jiang, Y. Zhang, S. V. Morozov, H. L. Stormer, U. Zeitler, J. C. Maan, G. S. Boebinger, P. Kim, A. K. Geim, *Science* **315**, 1379 (2007).
 - [5] A. H. Castro Neto, F. Guinea, N. M. R. Peres, K. S. Novoselov, and A. K. Geim, *Rev. Mod. Phys.* **81**, 109 (2009).
 - [6] M. Mucha-Kruczynski, E. McCann and V. I. Falko, *Semicond. Sci. Technol.* **25**, 033001 (2010).
 - [7] Xiao-Liang Qi and Shou-Cheng Zhang, *Rev. Mod. Phys.* **83**, 1057, (2011).
 - [8] A. A. Burkov and L. Balents, *Phys. Rev. Lett.* **107**, 127205, (2011).
 - [9] S. Das Sarma, S. Adam, E. H. Hwang, and E. Rossi, *Rev. Mod. Phys.* **83**, 407 (2011).
 - [10] A. K. Geim and A. H. MacDonald, *Phys. Today* **60** (8), 35 (2007).
 - [11] J. G. Checkelsky, Lu Li, and N. P. Ong, *Phys. Rev. Lett.* **100**, 206801 (2008).
 - [12] D. A. Abanin, K. S. Novoselov, U. Zeitler, P. A. Lee, A. K. Geim, and L. S. Levitov, *Phys. Rev. Lett.* **98**, 196806 (2007).
 - [13] M. König, S. Wiedmann, C. Brune, A. Roth, H. Buhmann, L. W. Molenkamp, X.-L. Qi, and S.-C. Zhang, *Science*, **318**, 766 (2007).
 - [14] D. A. Abanin, S. V. Morozov, L. A. Ponomarenko, R. V. Gorbachev, A. S. Mayorov, M. I. Katsnelson, K. Watanabe, T. Taniguchi, K. S. Novoselov, L. S. Levitov, A. K. Geim, *Science* **332**, 328 (2011).
 - [15] J. Renard, M. Studer, and J. A. Folk, *Phys. Rev. Lett.* **112**, 116601 (2014).
 - [16] A. F. Young, J. D. Sanchez-Yamagishi, B. Hunt, S. H. Choi, K. Watanabe, T. Taniguchi, R. C. Ashoori and P. Jarillo-Herrero, *Nature*, **505**, 528 (2014).
 - [17] P. Maher, C. R. Dean, A. F. Young, T. Taniguchi, K. Watanabe, K. L. Shepard, J. Hone and P. Kim, *Nature Physics*, **9**, 154 (2013).
 - [18] B. Büttner, C. X. Liu, G. Tkachov, E. G. Novik, C. Brne, H. Buhmann, E. M. Hankiewicz, P. Recher, B.

- Trauzettel, S. C. Zhang, and L. W. Molenkamp, *Nature Phys.* **7**, 418 (2011).
- [19] D. A. Kozlov, Z. D. Kvon, N. N. Mikhailov, and S. A. Dvoretiskii, *JETP Letters*, **96**, No. 11, 730 (2012).
- [20] D. A. Kozlov, Z. D. Kvon, N. N. Mikhailov, and S. A. Dvoretiskii, *JETP Letters*, **100**, No. 11, 724 (2014).
- [21] H. Buhmann, *Journal. Appl.Phys.*, **109**, 102409 (2011).
- [22] G. M. Gusev, Z. D. Kvon, O. A. Shegai, N. N. Mikhailov, S. A. Dvoretzky and J. C. Portal, *Phys. Rev. B* **84**, 121302(R) (2011).
- [23] Z. D. Kvon, E. B. Olshanetsky, and D. A. Kozlov et al., *Pisma Zh. Eksp. Teor. Fiz.* **87**, 588 (2008) [*JETP Lett.* **87**, 502 (2008)].
- [24] E. B. Olshanetsky, Z. D. Kvon, N. N. Mikhailov, E. G. Novik, I. O. Parm, and S. A. Dvoretzky, *Solid State Commun.* **152**, 265 (2012).
- [25] See Supplemental Material, which includes Ref.12 for details on the conductivities measurements and the model that take into account the edge and bulk contribution to the total current in Dirac metal at $\nu = 0$ LL.
- [26] S. Das Sarma, Kun Yang, *Solid State Commun.* **149**, 1502 (2009).
- [27] E. B. Olshanetsky, Z. D. Kvon, G. M. Gusev, A. D. Levin, O. E. Raichev, N. N. Mikhailov, S. A. Dvoretzky, *Phys.Rev.Lett.*, **114**, 126802 (2015).
- [28] Y. Barlas, Kun Yang and A. H. MacDonald, *Nanotechnology* **23**, 052001, 20 (2012).
- [29] J. N. Fuchs and P. Lederer, *Phys. Rev. Lett.* **98**, 016803 (2007).
- [30] K. Nomura, S. Ryu and D. H. Lee, *Phys. Rev. Lett.* **103**, 216801 (2009).
- [31] C. Y. Hou, C. Chamon, and C. Mudry, *Phys. Rev. B* **81**, 075427 (2010).
- [32] I. A. Lukyanchuk and A. M. Bratkovsky, *Phys. Rev. Lett.* **100**, 176404 (2008).
- [33] G. M. Gusev, E. B. Olshanetsky, Z. D. Kvon, A. D. Levin, N. N. Mikhailov, and S. A. Dvoretzky, *Phys. Rev. Lett.* **108**, 226804 (2012).
- [34] B. Scharf, A. Matos-Abiague, and J. Fabian, *Phys. Rev. B* **86**, 075418 (2012).
- [35] J.-C. Chen, J. Wang, and Q.-F. Sun, *Phys. Rev. B* **85**, 125401 (2012).
- [36] M. V. Durnev and S. A. Tarasenko, *Phys.Rev. B* **93**, 075434 (2016).
- [37] O. E. Raichev, *Phys.Rev B* **85**, 045310 (2012).